JOURNAL OF PROPULSION AND POWER
Vol. 23, No. 1, January–Febrary 2007

Technical Notes

TECHNICAL NOTES are short manuscripts describing new developments or important results of a preliminary nature. These Notes should not exceed 2500 words (where a figure or table counts as 200 words). Following informal review by the Editors, they may be published within a few months of the date of receipt. Style requirements are the same as for regular contributions (see inside back cover).

Method for Aerodynamic Analysis of Wind Turbines at Peak Power

Sven Schmitz* and Jean-Jacques Chattot†
University of California, Davis, Davis, California 95616-5294

DOI: 10.2514/1.18318

I. Introduction

In 2005, global wind-power capacity surpassed the 50-GW mark. Since 1990, the wind industry is the fastest growing energy source in the world, with an average annual growth rate of more than 26% [1]. The success of wind power as an alternate energy source is closely related to the economics of wind-power production. An improved understanding of the aerodynamics underlying wind turbines will optimize blade design and maximize power output.

In April 2000, the National Renewable Energy Laboratory (NREL) conducted the phase 6 experiment in the NASA Ames Research Center's 80×120 ft wind tunnel [2]; see Fig. 1a. The NREL phase 6 rotor is a two-bladed, stall-controlled wind turbine equipped with the S809 airfoil [3,4]. Measured rotor torque vs wind speed is shown in Fig. 1b. As opposed to pitch-controlled wind turbines, stall-controlled wind turbines such as the NREL phase 6 rotor achieve a passive power control by allowing local airfoil sections to stall. For the NREL phase 6 rotor and $9 \text{ m/s} < V_{\text{Wind}} < 20 \text{ m/s}$, the balance between increasing available wind power and increased drag due to sectional airfoil stall achieves a nearly constant power output. Stall that is initiated inboard, progresses outboard along the blade span, causing decreased lift and increased drag. Strong 3-D effects are present, which are difficult to predict with computational models.

During the course of the phase 6 experiment, NREL invited aerodynamic modelers to participate in a blind comparison study to compare and validate state-of-the-art computational models. Four different classes of models participated (i.e., performance codes, wake codes, aeroelastic codes, and CFD codes). In December 2000, predictions were presented and compared with measured wind-tunnel data [5]. Large discrepancies between predictions and measurements were found. Modelers were indeed disappointed that predictions for a typical wind turbine operating condition (no-yaw, steady-state, and no-stall) at $V_{\text{Wind}} = 7 \text{ m/s}$ ranged from 25–175% of measured data. At higher wind speeds of $V_{\text{Wind}} > 9 \text{ m/s}$, power predictions ranged from 30–275% and deviated even more from measured data. Participants attributed discrepancies observed to different modeler assumptions on how to use the 2-D airfoil data [3] to account for rotational and 3-D effects. One full-domain CFD analysis gave the best predictions over the entire power range among all other computational models [6]. However, this code was numerically very expensive (greater than 3.0×10^6 nodes) and still failed to accurately predict the peak power aerodynamics of the NREL phase 6 rotor at $V_{\text{Wind}} = 9 \text{ m/s}$. Leishman [7] has discussed fundamental limits in all computational models and how this still challenges the understanding of wind turbine flow physics today.

This paper focuses on the 3-D flow phenomena of the NREL phase 6 rotor occurring at wind speeds close to peak power and peak torque at $V_{\text{Wind}} = 9 \text{ m/s}$ (Fig. 1b). Here, the blade operates just at the onset of radial pumping, stall delay, and spiral separation. Recently, the flow physics of such 3-D vortical flows that lead to force amplification and delayed stall has been revisited by Schreck and Robinson [8] and Tangler [9] analyzing NREL measurements. In this work, two computational models are compared: a vortex line model (VLM) and a parallelized coupled solver (PCS) consisting of a Navier–Stokes (NS) zone in the near field and a vortex method in the far field. It is found that the PCS method gives insight into the peak power aerodynamics of stall-controlled wind turbines, at an affordable computational expense. This makes PCS a potential method for future development and design of stall-controlled wind turbines.

II. Numerical Methods

A. Vortex Line Model

This model consists of a lifting line and a rigid wake; see Chattot [10] for a detailed description. The rigid wake is formed by a helicoidal vortex sheet for which the pitch is determined such that the wake is in equilibrium, in the sense that the absorbed power in the far wake matches the rotor power. The high sectional Reynolds numbers of 10^5–10^6 along the blade ensure that vortical structures are indeed convected far downstream behind the rotor blade (see Fig. 1a). The roll-up of the vortex sheet and increase in stream tube diameter behind the rotor are not accounted for. For slowly rotating wind turbines and small yaw angles, both are second-order effects that do not alter the total vorticity content but only redistribute it slightly in space. Good results are obtained for fully attached and moderately separated flow. However, VLM evaluates local lift and drag coefficients $C_{L,j}$ and $C_{D,j}$ at each radial section j from a single 2-D viscous polar. Thus, it does not account for spanwise flow gradients such as those associated with 3-D effects in large separated regions.

B. Parallelized Coupled Solver

PCS has been developed [11] to reduce both numerical dissipation of vortical structures and computational cost compared with a full-domain NS analysis. The near field is solved with a commercial NS solver (CFX-5.6 by ANSYS, Inc.), assuming steady and fully turbulent conditions using the κ-ω two-equation turbulence model. The steady flow assumption is supported by NREL measurements at zero yaw [2] and previous steady results of a full-domain NS analysis [6]; the fully turbulent flow assumption currently limits the PCS method from accurately predicting the local onset and amount of separation and stall at higher wind speeds. The far field is predicted with a rigid wake model, VLM. An illustration is given in Fig. 2. The

Presented as Paper 4850 at the 23rd AIAA Applied Aerodynamics Conference, Toronto Ontario, Canada, 6–9 June 2005; received 20 June 2005; revision received 29 September 2006; accepted for publication 19 September 2006.

*Post-Graduate Researcher, Department of Mechanical and Aeronautical Engineering, One Shields Avenue; shschmitz@ucdavis.edu. Member AIAA.
†Professor and Chair, Department of Mechanical and Aeronautical Engineering, One Shields Avenue; jjchattot@ucdavis.edu. Member AIAA.

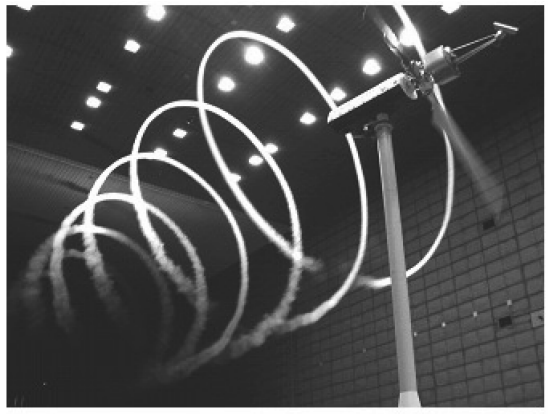

a)

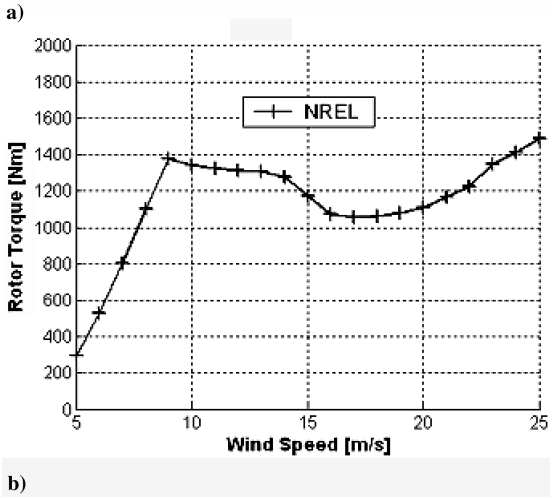

b)

Fig. 1 NREL phase 6 rotor (courtesy of NREL).

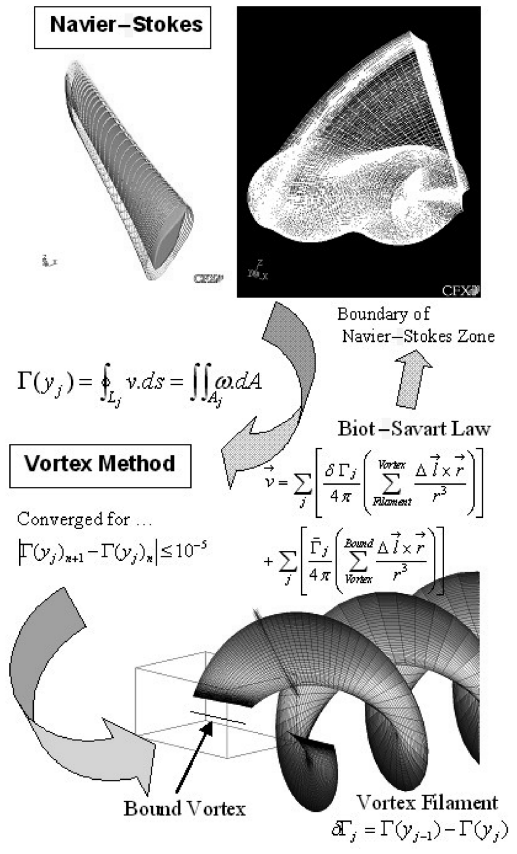

Fig. 2 Parallelized coupled solver.

NS solver is parallelized on a cluster of four processors. Near-wall treatment is handled by scalable wall functions in CFX-5.6, with $20 < y^+ < 90$ for all cases. The NREL phase 6 rotor blade is meshed with 120 points along its contour and 40 points in the spanwise direction. A grid-independence study was performed in 2-D for the S809 airfoil, showing consistent results [12]. The actual tip shapes of the NREL phase 6 rotor [2] are not modeled. Blunt blade tips are meshed with an unstructured Delaunay surface mesher and extruded as prisms to the boundaries of the NS zone. A critical feature of the present method is that the wake surface is aligned with the first 60 deg of azimuth of the vortex sheet created by VLM, such that vortex filaments in Fig. 2 pass between nodes. This allows for an efficient capture of the NS wake and ensures that induced velocities obtained by VLM are smooth along the boundary of the NS zone by avoiding the close proximity of boundary nodes to vortex filament singularities. The NS zone extends to 1–3 reference chord lengths around the blade and 3–6 reference chord lengths into the wake (see also Fig. 2). The hybrid mesh inside the NS zone contains a total of approximately 880,000 nodes.

The coupling methodology of PCS is shown in Fig. 2. Starting with an undisturbed flow consisting of wind speed and blade rotation entrainment speed, the NS code solves for the flowfield around the wind turbine blade. Inside the NS region, the circulation at each radial station is determined by performing a closed line integral with the contour L_j, including all sources of vorticity according to Stokes's theorem. The vortex method distributes Γ_j along a bound vortex and distributes the trailing vorticity $\delta\Gamma_j$ along a rigid wake, using a symmetry condition for two rotor blades. Induced velocities are calculated by a discrete form of the Biot–Savart law and are imposed as boundary conditions to the NS region for the next coupling step. Coupling is performed after each 10–20 accumulated time steps of the NS solver. The coupling is considered to be converged if the change in Γ_j is less than 10^{-5}. This is usually achieved after 3–5 coupling steps [11,12].

III. Results and Discussion

Results presented in this work correspond to an upwind case (S sequence) of the NREL phase 6 experiment with the rotor being in steady and no-yaw conditions at a blade pitch of $\phi = 3$ deg [2]. VLM and PCS were applied for wind speeds surrounding peak torque in Fig. 1b. Results obtained for the integrated rotor torque are shown in Fig. 3. Very good agreement is found between experiment and computations for fully attached flow, $V_{\text{Wind}} = 7$ m/s. Both computational models underpredict peak power and torque at $V_{\text{Wind}} = 9$ m/s by approximately 10%. For $V_{\text{Wind}} > 9$ m/s, the rotor torque predictions start to follow different trends, with the VLM code overpredicting post-peak torque.

The spanwise bound circulation Γ_j is the basic quantity for the VLM code and the coupling methodology in PCS (see Fig. 2). Results obtained for Γ_j are shown in Figs. 4a and 4c. Note that $\delta\Gamma_j$ is associated with trailing vorticity that is attached to filament j. In

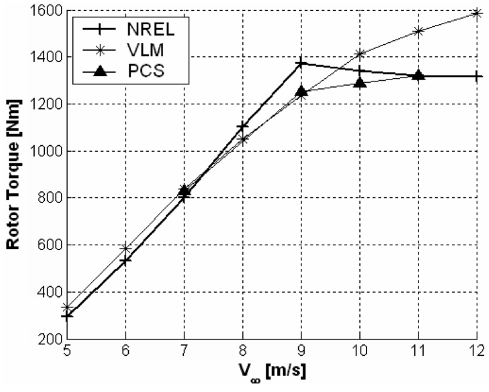

(NREL Phase 6 Rotor, S-Sequence)

Fig. 3 Measured and computed rotor torque.

Figs. 4a and 4c, the root vortex shows $\delta\Gamma_j < 0$ and the tip vortex $\delta\Gamma_j > 0$. In Fig. 4b, values for the PCS computed coefficient of lift $C_{L,j}$ were obtained using the Kutta–Joukowski lift theorem as $C_{L,j} = -2\Gamma_j/(U_{\infty,j} \cdot c_j)$, where c_j is the local blade chord and $U_{\infty,j}$ is the local freestream speed obtained from the ambient pressure p_∞ and the local stagnation pressure $p_{\text{stag},j}$ using the incompressible Bernoulli equation.

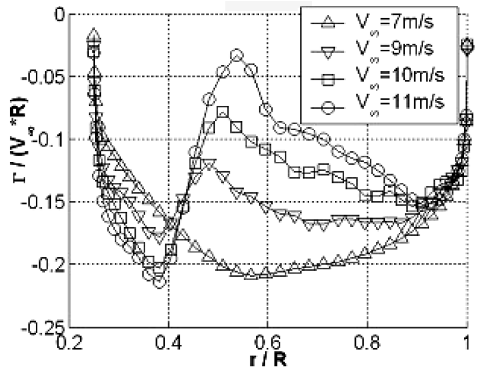

a) PCS

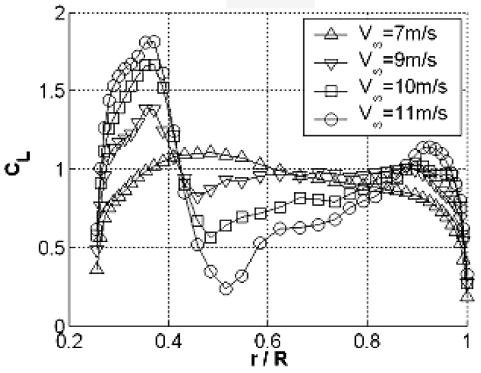

b) PCS

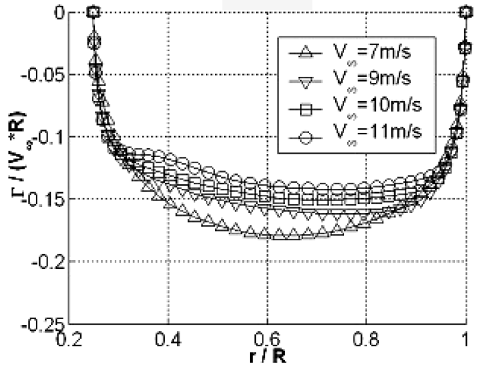

c) VLM

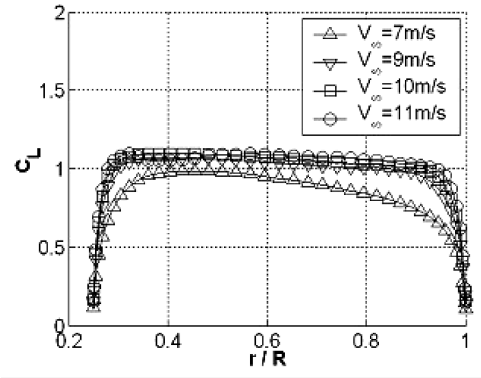

d) VLM

Fig. 4 Spanwise circulation and lift coefficient (PCS and VLM).

For $V_{\text{Wind}} = 7$ m/s, comparison between VLM and PCS in Fig. 4 with respect to Γ_j and $C_{L,j}$ reveals the presence of 3-D boundary-layer effects for attached flow [11]. For $V_{\text{Wind}} > 7$ m/s, Fig. 4a illustrates a region of $\delta\Gamma_j > 0$ between $0.4 < r/R < 0.5$ that

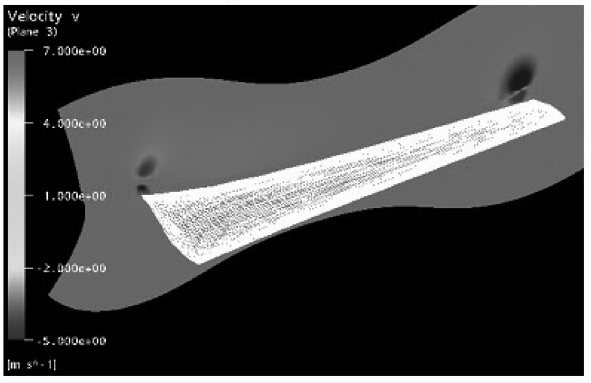

a) V=7 m/s

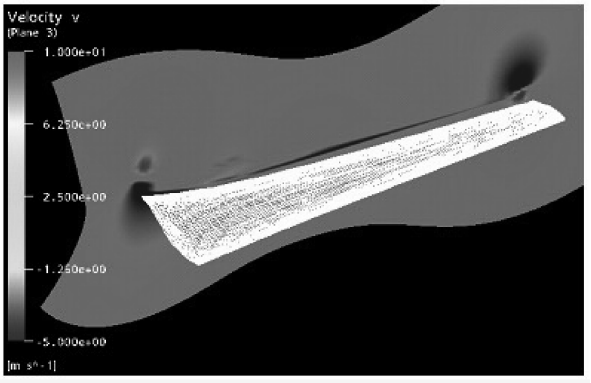

b) V=9 m/s

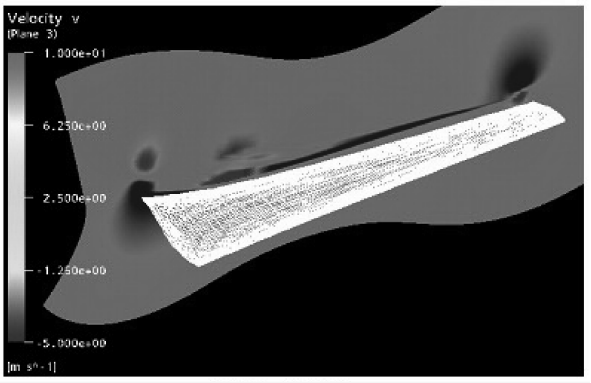

c) V=10 m/s

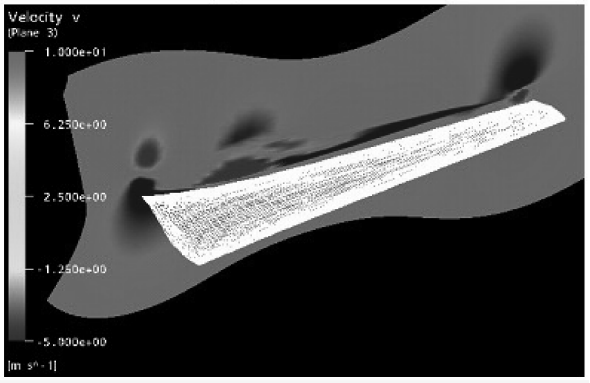

d) V=11 m/s

Fig. 5 Velocity *v* in spanwise direction behind the rotor blade (PCS).

increases both in radial extent and value for increasing wind speed. This cannot be observed for VLM results in Fig. 4c. As far as local values for the coefficient of lift $C_{L,j}$ are concerned, they are shown in Fig. 4b for the PCS runs and in Fig. 4d for the VLM runs. Figures 4b and 4d illustrate that the 2-D maximum $C_{L,j}$ of approximately 1.1 is far exceeded [3] in the 3-D PCS runs for $V_{\text{Wind}} > 7$ m/s. Furthermore, PCS results for $C_{L,j}$ show a rapid drop following its peak, indicating separated and stalled flow along the blade. The VLM code is limited to a single 2-D viscous polar, which cannot predict such 3-D stall delay effects. The large discrepancies in spanwise circulation Γ_j between VLM and PCS give rise to further investigation of the flow physics. In particular, the $\delta\Gamma_j > 0$ region between $0.4 < r/R < 0.5$ indicates the presence of a vortex that causes separation on the upper surface of the blade. This vortex is first initiated by increased radial flow in a small separated region prior to peak power at $V_{\text{Wind}} = 9$ m/s. Figure 5 illustrates the spanwise velocity component v in a plane located between 5–10% of the average chord downstream of the blade's trailing edge. The view is of the upper blade surface, with the blade root on the left and the blade tip on the right. Note that the large $\delta\Gamma_j$ in Fig. 4a can be illustrated in Fig. 5 by means of the spanwise velocity component v. Figure 5d shows a vortex associated with concentrated trailing vorticity $\delta\Gamma_j$ rotating in opposite sense to the root vortex. The 3-D effect can be observed as a downwash inboard of the vortex that results in a stall delay and an upwash outboard of it that enhances stall. The balance between these two effects achieves a nearly constant rotor power for $9 \text{ m/s} < V_{\text{Wind}} < 14$ m/s. This highly 3-D flow feature cannot be captured with VLM, because this method only matches blade axial and azimuthal flow conditions with 2-D airfoil data. Recently, the authors also detected the vortex in the absence of rotational influences by applying the PCS method to the parked phase 6 rotor [13] at high pitch angles. However, the vortex was seen more inboard at $r/R = 0.40$. As for the PCS results in the present work under rotating conditions, the Coriolis force acts toward the upper-surface trailing edge at the blade root [14] (Himmelskamp effect) and thus decreases the adverse pressure gradient, which further delays stall inboard of the vortex. Therefore, the vortex is located more outboard for the rotating case. The PCS method yields the correct 3-D bound circulation Γ_j as required by Stokes's theorem.

IV. Conclusions

A parallelized coupled solver has been applied to the stall-controlled NREL phase 6 rotor near peak power for assessing the effect of 3-D physical phenomena. Comparison of PCS results with a vortex line method showed major discrepancies in the spanwise bound circulation Γ_j and local lift coefficient $C_{L,j}$. A vortex forming on the upper blade surface affects the distribution of bound circulation and creates an area of concentrated vorticity traceable with the spanwise velocity component v. The PCS method has proven its potential for delineating the 3-D vortical flow phenomena occurring near peak power/torque of the NREL phase 6 rotor. The coupling of a near-field NS solver with a far-field wake model proved to be a useful predictive tool for future analysis of wind turbine aerodynamics and the design of stall-controlled wind turbines. Furthermore, it is computationally more efficient than a conventional full-domain NS analysis. In addition, it significantly reduces the numerical dissipation associated with the presence of vortical structures.

References

[1] Anon., "Global Wind 2005 Report" [online report], Global Wind Energy Council (GWEC), http://www.gwec.net/fileadmin/documents/Publications/Global_WindPower_05_Report.pdf [retrieved 20_Oct_2006].

[2] Hand, D. M., Simms, D. A., Fingersh, L. J., Jager, D. W., Cotrell, J. R., Schreck, S., and Larwood, S. M., "Unsteady Aerodynamics Experiment Phase 6: Wind Tunnel Test Configurations and Available Data Campaigns," National Renewable Energy Laboratory Rept. TP-500-29955, Dec. 2001.

[3] Somers, D. M., "Design and Experimental Results for the S809 Airfoil," National Renewable Energy Laboratory Rept. SR-440-6918, 1997.

[4] Giguere, P., and Selig, M. S., "Design of a Tapered and Twisted Blade for the NREL Combined Experiment Rotor," National Renewable Energy Laboratory Rept. SR-500-26173, 1999.

[5] Simms, D., Schreck, S., Hand, M., and Fingersh, L. J., "NREL Unsteady Aerodynamics Experiment in the NASA-Ames Wind Tunnel: A Comparison of Predictions to Measurements," National Renewable Energy Laboratory Rept. TP-500-29494, 2001.

[6] Sorensen, N. N., Michelsen, J. A., and Schreck, S., "Navier–Stokes Predictions of the NREL phase 6 Rotor in the NASA Ames 80 ft × 120 ft Wind Tunnel," *Wind Energy Technology*, Vol. 5, No. 2, 2002, pp. 151–169.

[7] Leishman, J. G., "Challenges in Modeling the Unsteady Aerodynamics of Wind Turbines," AIAA Paper 2002-0037, Jan. 2002.

[8] Schreck, S., and Robinson, M., "Boundary Layer State and Flow Field Structure Underlying Rotational Augmentation of Blade Aerodynamic Response," *Journal of Solar Energy Engineering*, Vol. 125, No. 4, 2003, pp. 448–456.

[9] Tangler, J. L., "Insight into Wind Turbine Stall and Post-Stall Aerodynamics," *Wind Energy Technology*, Vol. 7, No. 3, 2004, pp. 247–260.

[10] Chattot, J. J., "Design and Analysis of Wind Turbines Using Helicoidal Vortex Model," *Computational Fluid Dynamics Journal*, Vol. 11, No. 1, 2002, pp. 50–54.

[11] Schmitz, S., and Chattot, J. J., "A Coupled Navier–Stokes/Vortex-Panel Solver for the Numerical Analysis of Wind Turbines," *Computers and Fluids*, Vol. 35, No. 7, 2006, pp. 742–745.

[12] Schmitz, S., "Coupling of Navier–Stokes Solver with Helicoidal Vortex Model for the Computational Study of HAWTs," Ph.D. Dissertation, Univ. of California, Davis, Davis, CA, 2006, Chap. 3.2.4.

[13] Schmitz, S., and Chattot, J. J., "Characterization of Three-Dimensional Effects for the Rotating and Parked NREL Phase 6 Wind Turbine," AIAA Paper 2006-0392, Jan. 2006.

[14] Du, Z., and Selig, M. S., "The Effect of Rotation on the Boundary Layer of a Wind Turbine Blade," *Renewable Energy*, Vol. 20, No. 2, 2000, pp. 167–181.

C. Tan
Associate Editor